Journal of Environmental Health Science and Engineering (2023) 21:167–185
https://doi.org/10.1007/s40201-023-00851-4

RESEARCH ARTICLE

Antimicrobial, antioxidant, cytotoxicity and photocatalytic performance of Co doped ZnO nanoparticles biosynthesized using *Annona Muricata* leaf extract

P. S. Vindhya[1] · Sandhya Suresh[1] · R. Kunjikannan[2] · V. T. Kavitha[1,3]

Received: 19 June 2022 / Accepted: 25 January 2023 / Published online: 3 February 2023

Abstract
In the present study, ZnO nanoparticles doped with 3%, 5% and 7% of cobalt have been synthesized by green method using *Annona muricata* leaf extract. The obtained nanopowder was characterised by XRD, FTIR, XPS, HRTEM, SAED, SEM, EDAX and UV–Visible spectroscopy techniques. XRD patterns confirm the formation of pure and Co doped ZnO nanoparticles with a hexagonal wurtzite structure with high phase purity. FTIR spectra indicate the stretching vibration of Zn–O at 495 cm^{-1}. The incorporation of Co^{2+} ions into the ZnO lattice was identified by XPS analysis. EDX spectra confirm the existence of Co, Zn and O elements. The SEM and HRTEM micrographs show morphology of nanoparticles. The optical study specifies a decrease in energy band gap with an increase in Co-doping concentration. The photocatalytic performance of ZnO and $Zn_{0.93}Co_{0.07}O$ has been examined for the degradation of methylene blue (MB) under sunlight irradiation. The antimicrobial activity of synthesized nanoparticles against *s.aureus*, *p.aeruginosa*, *b.subtilis* bacterial strains *c.albicans* and *a.niger* fungal strains as investigated. The $Zn_{0.93}Co_{0.07}O$ nanoparticles exhibit good antioxidant properties. Moreover, the cytotoxicity of ZnO nanoparticles was evaluated against L929 normal fibroblast cells. So, this work suggests that *Annona muricata* leaf extract mediated pure and Co-doped ZnO nanoparticles are a potential candidate for biomedical and photocatalytic applications.

Keywords ZnO nanoparticles · Green synthesis · Antimicrobial · Antioxidant · Cytotoxicity · Photocatalytic activity

Introduction

Microbial infections are serious health issues for living organism, which causes huge morbidity, millions of causalities and mortality is an emerging public health issue across the globe level, demands the development of effective antimicrobial resistance [1]. However, the discovery of novel medical drug with increase in antimicrobial action is expanding challenge to scientific community [2]. In this scenario, the antibiotic medications and lack of novel strategically actions are needed for the development of new antimicrobial resistance for the treatments in different pathway [3]. Nanomaterials have small size and large surface to volume ratio, can generate reactive oxygen species which induce high oxidative stress and destroy cell membranes, DNA, protein formation, thus leads to microbial cell death [4].

Now a days, rapid industrialization as well as rapid population growth result in environmental pollution and a scarcity of pure fresh water [5]. About 1.8 million children were euthanized each year as a consequence of water related diseases [6]. Water scarcity affects approximately half of the world's population and nearly 20% of textile effluents contain colorants, which are a major contributor to river pollution [7]. The synthetic dye effluents that are used as major colouring agents in food, cosmetic, textile, paper, printing and leather industries are non-degradable in nature and release a large number of toxic pollutants into aquatic water, leading to harmful diseases for human health and aquatic life through eutrophication [8]. MB ($C_{16}H_{18}N_3SCl$) is a

✉ V. T. Kavitha
kavithamgcollege@gmail.com

[1] Post Graduate and Research Department of Physics, Mahatma Gandhi College, University of Kerala, Thiruvananthapuram 695004, Kerala, India

[2] Department of Physical Education, University College, Thiruvananthapuram 695034, Kerala, India

[3] NSS College for Women, University of Kerala, Thiruvananthapuram 695040, Kerala, India

cationic azo dye used in paper, silk fabric, printing, colouring and as a chemical reagent in dying that causes vomiting, breathing problems, hyperhidrosis and nervous disorders [9]. On a large scale industry, the dye has been effectively decomposed into organic pollutants in a reliable, low cost, non-destructive, low energy consumption, high efficiency, eco-friendly purification using biological treatments that has become a major focus for scientists [10]. Different advanced oxidation processes like coagulation, osmosis, filtration, ion exchange, precipitation and photodegradation are in practise for the efficient removal of dyes from contaminated water [11]. Out of various approaches, heterogeneous photocatalysis is one of the major and most validated treatment for the removal of dye pollutants, favoured for their operating features of cost effectiveness, eco-friendliness, low energy consumption, independence from secondary chemicals, and easye of operation [12]. Sustainable photocatalytic process involving light energy as a renewable source of energy to activate photocatalysts such as metal or semiconductor nanoparticles to degrade environmentally hazardous pollutants [13].

To date, metal oxide nanoparticles displaying large surface area and multifunctional properties have received immense attention in everyday life applications like sports textiles, agriculture, energy and health care industries [14]. The characteristic advantages of high biocompatibility, biodegradability, easy availability and the interaction of biomolecules are easy adaptation and flexibility in drug delivery [15]. ZnO is a well-known n-type II-IV semiconductor material with a wide band gap (3.37 eV) and high electron–hole binding energy (60 MeV) [16]. The structural, morphological and biological properties of ZnO nanoparticles have received remarkable interest in cosmetics, odour control [17], surface coatings and antimicrobial agents in sports textiles [18]. The properties of ZnO nanoparticles were enhanced by effective doping with transition metals like Mn [19], Fe [20], Mg [21], Co [22], Al [23] and Ni. This created lattice defects, changes in surface area, and surface oxygen vacancies, which provided an extra path for electronic transitions by tailoring the bandgap as well as generating defects in the band structure [24]. Among the transition metals, cobalt dopant can enhance recombination centres, surface area, crystal structure, shape and size, which allows for excellent material for well-organized antimicrobial and photo catalytic agents [25].

ZnO nanoparticles can be prepared by different chemical and physical techniques that utilise high energy, high cost, non-polar solvents, high radiation and toxic chemicals [26]. Bio-inspired agents reduces the generation of hazardous waste and toxic substances in the environment while producing high purity, less toxic, low cost and eco-friendly nanomaterials [27]. Phytochemicals present in the plants are "natural chemical factories" [28], acting as natural capping, reducing, oxidizing and stabilizing agent [29]. The flavonoids, phenols, alkaloids and vitamins present in the *A.muricata* leaf extract exhibit good antibacterial, antioxidant and cytotoxic properties [30]. For this reason, the present study was performed for the green synthesis of ZnO and cobalt doped ZnO nanoparticles using *Annona Muricata* leaf extract for the very first time. The synthesised nanoparticles were analysed by various characterization techniques. Moreover, the *in-vitro* cytotoxicity, antioxidant, antibacterial, antifungal and photocatalytic activities of nanoparticles were performed for the degradation of methylene blue dye in an aqueous medium.

Experimental procedures

Materials

Fresh leaves of *A.muricata* were collected from home in Thiruvananthapuram, Kerala, India. Without further purification, $Zn(NO_3)_2.6H_2O$, $Co(NO_3)_2.6H_2O$ and NaOH were purchased from Sigma Aldrich, India (purity: 99.99%). Methylene blue (MB) dye was obtained from Nice chemicals, and double distilled water is used as a solvent throughout the experiment.

Plant materials and its preparation

A.muricata fresh leaves were collected and washed thoroughly with tap water and double distilled water. Subsequently, 25 g of leaves were cut into fine pieces and boiled at 60 ℃ in 250 ml of double distilled water. The aqueous solution turns light brownish yellow after boiling. Now the leaf extract is allowed to cool, and then it is filtered with Whatman no.42 filter paper. The filtered leaf extract was stored for the preparation of nanoparticles.

Synthesis of pure and Co doped ZnO nanoparticles

For the preparation of pure and Co doped ZnO, the calculated the stoichiometric ratio of Zinc nitrate and Cobalt nitrate ($Zn_{1-x}Co_xO$ (where x = 0.0, 0.03, 0.05 and 0.07)) was added to 30 ml of leaf extract and stirrer for 15 min. The pH 10 of the solution was maintained by adding NaOH solution in drop by drop, and the process was done at room temperature. The stirring process was continued for 3 h. Subsequently, the solution is centrifuged and filtered through Whatman No. 42 filter paper. The filtered precipitate is placed in a hot air oven at 100˚C and annealed at 500˚C for 2 h. The synthesis process of nanoparticles is shown in Fig. 1. The obtained nanopowder was ground into

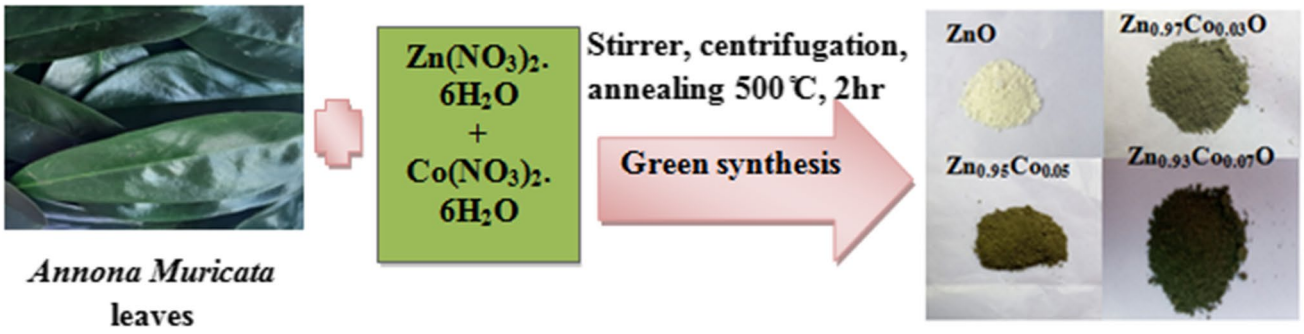

Fig. 1 Synthesis of 0%, 3%, 5% and 7% Co doped ZnO nanoparticles

a fine powder and kept for further characterizations and applications.

Characterizations

XRD patterns were recorded using a D8 Advance Bruker X-ray diffractometer equipped with a CuKα radiation source. The functional groups present in the material are identified using FTIR spectra and recorded using Thermo Nicolet Avatar 370. XPS measurements were done by a Thermo Scientific ESCALAB Xi + X-ray Photoelectron spectrometer. The morphology of samples was employed by HR-TEM images along with the SAED pattern using JEOL/JEM 2100. The surface morphology was analysed by SEM JEOL 6390LA and the elemental composition of the samples was analysed by EDX spectra using OXFORD XMXN. The optical properties of nanoparticles were studied using a Perkin Elmer Lambda 365 spectrometer. The XRD, FTIR, XPS and UV–Visible spectra was plotted using origin 8.0 software (Origin Lab Corporation, USA). Antimicrobial activity was analysed by measuring the diameter of the zone of inhibition and the cytotoxicity of were calculated using ED50 PLUS V1.0 software.

Antibacterial activity

The antimicrobial activities of $Zn_{1-x}Co_xO$ (x = 0.0, 0.03, 0.05 and 0.07) nanoparticles against gram positive (*Bacillus subtilis (MTCC*2413*)*, *Staphylococcus aureus (MTCC* 87*))* and gram negative (*Pseudomonas aeruginosa (MTCC* 741*)* pathogenic bacteria were evaluated using the Agar well diffusion method. Mueller–Hinton agar medium (HIMEDIA- M173) of 15–20 ml was poured on petri plates and allowed to solidify. Standardized inoculums were uniformly spread on the surface, and four wells with a diameter of 9 mm (20 mm apart from one another) were pressed with sterile cork borer. Nanopowder with a concentration of 40 and 80 µL from 10 mg/ml was added into the wells in T1 & T2 forms. Gentamycin (40 µl from 4 mg/ml stock) is added to the positive well (+) and the sample dilution solvent is added to the negative well (-). The plates were incubated under aerobic conditions, and after incubation, the zone of bacterial growth inhibition around wells was measured.

Antifungal activity

Potato dextrose agar plates were prepared and kept overnight. Grown species of *Candida albicans and* ***Aspergillus*** *Niger* fungus were swabbed. Wells of approximately 10 mm were bored using a well cutter and samples of different concentrations, such as 250 µg, 500 µg and 1000 µg were added. The plates were incubated at 37ºC for 24 h.Then the zone of inhibition was measured and compared with that of a standard antimycotic (Clotrimazole).

Antioxidant assay

The radical scavenging activity of nanoparticles was determined by a DPPH assay. The nanoparticles of different concentrations of 12.5, 25, 50, 100 and 200 µg/mL from the stock solution were made up to a final volume of 20 µl with DMSO and 1.48 ml DPPH (0.1 mM) solution were added. The reaction mixture was incubated in a dark environment at room temperature for 20 min. The absorbance readings were taken at 517 nm wavelength. The radical scavenging ability was tested, and the percentage of DPPH inhibition was calculated using the relation,

$$percentage\ of\ inhibition = \frac{A_{(Control)} - A_{(Test)}}{A_{(Control)}} * 100 \quad (1)$$

Cytotoxic studies

The L929 normal fibroblast cell lines were used for cytotoxic studies of prepared ZnO nanoparticles. L929 cells were cultured in 25cm^2 tissue in a culture flask. The cultured cell

lines are kept at 37℃ in a humidified 5% CO_2 incubator. The cell viability was evaluated by direct observation of cells by MTT assay. After incubation of 24 h, the sample content was separated from the well and 30 µl of MTT solution was added to control wells and test samples followed by incubation at 37℃ for 4 h. After removing the supernatant, 100 µl of dimethyl sulfoxide solution is added. The wells are mixed gently by pipetting up and down to solubilize the formazan crystals. The absorbance values are measured using a microplate reader having a wavelength of 550 nm. The viability percentage is calculated using the formula,

$$\% \ viability = \frac{ODtest}{OD \ control} * 100 \quad (2)$$

Photocatalytic study

The photocatalytic performance of pure and Co doped ZnO nanoparticles was tested by methylene blue (MB). The dye solution at a concentration of 100 mg/L was prepared and stirred in dark conditions for 1 h to reach adsorption–desorption equilibrium. The experiment was carried out in direct sunlight (10/01/2022, Time: 11 a.m to 1 p.m at Thiruvananthapuram, Kerala). For the photocatalytic study, 100 mg of catalyst was added to 100 ml of prepared dye solution and magnetically stirred. During the reaction, 10 ml of solution from the beaker was extracted at certain time intervals, and the catalyst was separated by centrifugation at 5000 rpm at 8 min. The dye concentration was calculated by measuring the absorbance intensity ratio between the remains and the original dye solution using a UV–Visible spectrophotometer (Perkin Elmer Lambda 365).

Results and discussion

XRD analysis

Phase purity, crystallite size and orientation of 0%, 3%, 5% and 7% of Co doped ZnO nanoparticles were analysed by XRD, as illustrated in Fig. 2. The diffraction peak corresponds to (100), (002), (101), (102), (112), (103) and (112) crystal planes, revealing the hexagonal wurtzite structure of ZnO nanoparticles with space group of p63mc(JCPDS card file No: 36–1451) [31]. The enlarged image of (101) peak was given in inset of Fig. 2, which shows a slight shift in peak position when compared to ZnO. This shift in peak position indicates the incorporation of Co^{2+} ions into the ZnO lattice [32]. Compared with pure ZnO there are no structural changes and no additional phase-changes due to Co doping in ZnO, which indicates samples are highly pure and Co-ions are successfully occupied in the lattice site rather than the interstitial site [33]. Narrow diffraction peaks indicate all the synthesised nanoparticles are crystalline in nature. The occupation of Zn^{2+} (0.60Å) lattice by Co^{2+} (0.58Å) causes crystal defects due to a change in ionic radius, resulting in a decrease in crystalline quality, a decrease in lattice

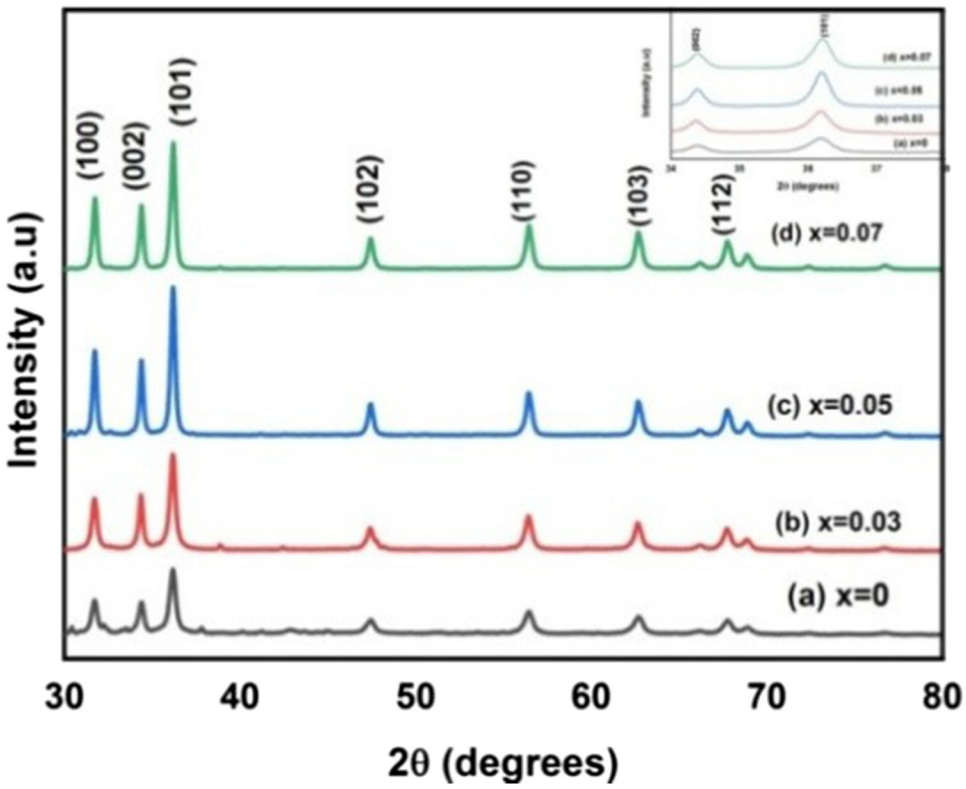

Fig. 2 XRD pattern of $Zn_{1-x}Co_xO$ (x = 0.0, 0.03, 0.05, and 0.07) nanoparticles

parameters, and an increase in lattice volume [34]. The change in peak intensity and full width half maximum could be attributed to c crystallite size and micro-strain.

In a hexagonal structure, the spacing between planes d can be calculated using the relation [35],

$$\frac{1}{d_{hkl}^2} = \frac{4}{3}\left\lfloor \frac{h^2 + hk + k^2}{a^2} \right\rfloor + \frac{l^2}{c^2} \tag{3}$$

Here, d_{hkl} is the interplanar distance corresponding to its miller indices of h, k, l planes, a and c are lattice constants.

The lattice constant a for (100) plane is calculated by,

$$a = \frac{\lambda}{\sqrt{3}\ \sin\ \theta_{100}} \tag{4}$$

The lattice constant c for (002) plane is calculated by,

$$c = \frac{\lambda}{\sin\ \theta_{002}} \tag{5}$$

The lattice parameters depend on concentration of dopant, defects in crystal structure, strain and ionic radii. Further, the changes in d-value, cell parameters, volume, bond-length, average crystallite size, shift in peak position and peak intensity confirm the substitution of Co in the ZnO lattice. Constant c/a ratios reveals that Co doping does not affect the hexagonal wurtzite structure of ZnO.

The volume of a unit cell is determined by the relationship,

$$\mathrm{v} = 0.866a^2c \tag{6}$$

a and c are lattice parameters. The volume of the unit cell (v) increases with the increase in Co doping indicated in Table 1. According to Vegard's law, the incorporation of Co^{2+} ions into the ZnO lattice could be identified by variations in the lattice constant and increase in volume of the unit cell, as well as the smaller ionic radius of the Co ion compared to Zn ions [36]. The Zn^{2+} has tetrahedral coordination, which is not completely filled by Co^{2+} in tetrahedral coordination [37]. Co^{2+} in octahedral coordination with r = 0.065 nm low spin and 0.075 nm high spin [38].

The crystalline size was calculated using the Debye–Scherrer equation,

$$D = \frac{K\lambda}{\beta\ \cos\ \theta} \tag{7}$$

where D is the mean size of crystallites (nm), K is crystallite shape factor, λ is the X-ray wavelength (1.5405 Å), β is the full width half maximum (FWHM) in radians of the X-ray diffraction peak and θ is the Bragg's angle.

The volume of nanoparticles is calculated by the relationship,

$$V = \frac{4}{3}\pi\left(\frac{D}{2}\right)^3 \tag{8}$$

The bond length (L) of Zn–O is calculated using the relation,

$$L = \sqrt{\left(\frac{a^2}{3} + \left(\frac{1}{2} - u\right)^2 c^2\right)} \tag{9}$$

u is the positional parameter and is calculated using the relation,

$$u = \left(\frac{a^2}{3c^2}\right) + 0.25 \tag{10}$$

Crystallographic defects are called dislocations or it's the length of dislocation lines per unit volume of the crystal. The dislocation density was calculated using the relation,

$$\delta = \frac{1}{\mathrm{D}^2} \tag{11}$$

The difference in crystallinity of nanoparticles is due to decrease in crystalline size and enhancement in dislocation density. Line broadening is caused by micro-strain and size. The slight increase in lattice parameters with increase in 'Co'

Table 1 Lattice parameters, Crystallite size, Volume of Unit cell, Volume of nanoparticles, positional parameter, bond length, dislocation density, Degree of distortion, Atomic Packing Fraction of $Zn_{1-x}Co_xO$ (x = 0.0, 0.03, 0.05 and 0.07) of nanoparticles

Sample		ZnO	$Zn_{0.97}Co_{0.03}O$	$Zn_{0.95}Co_{0.05}O$	$Zn_{0.93}Co_{0.07}O$
Lattice parameters	a(Å)	3.245	3.255	3.256	3.259
	c(Å)	5.199	5.216	5.218	5.219
$\frac{c}{a}$		1.6011	1.6024	1.6025	1.6014
Crystallite size (nm)		15	17	22	24
Volume of Unit cell $(Å)^3$		47.8252	47.8583	47.906	48.0036
Volume of nanoparticles		1766.25	2571.14	5572.45	7234.56
positional parameter (nm)		0.380015	0.379809	0.379789	0.379979
bond length (L) (Å)		1.98064	1.98108	1.98174	1.98311
dislocation density $(nm)^{-2}$		0.004444	0.00346	0.002066	0.001736
Degree of distortion		1.019245	1.019053	1.018976	1.019719
Atomic Packing Fraction		0.754372	0.75423	0.754173	0.754723

concentration into ZnO clearly shown in the data, which may be due to incorporation of Co ion on Zn site, which may be defined by the parameter, degree of distortion (R) as follows [39],

$$R = \frac{\left(2a\sqrt{\frac{2}{3}}\right)}{c} \tag{12}$$

If R = 1, confirms the ideal wurtzite structure as per the literature.

The Atomic Packing Fraction of Hexagonal structure was evaluated by the relation,

$$APF = \frac{2\pi a}{3\sqrt{3c}} \tag{13}$$

All the estimated lattice parameters, crystallite size, volume of unit cell, volume of nanoparticles, positional parameters, bond length, dislocation density, Degree of distortion, atomic packing fraction are tabulated in Table 1.

FTIR spectra

The functional group present in the materials has been identified by FTIR spectra, as shown in Fig. 3. The fundamental mode of vibration at 3440 cm^{-1} corresponds to O–H vibrational stretching mode [40]. The peak around 1361 cm^{-1} indicates the presence of H–O-H bending vibration, which may be due to water adsorbed in the nanoparticles during synthesis. The bond at 1066 cm^{-1} is due to C-O stretching vibration [41]. Furthermore, the band at 830 cm^{-1} corresponds to the formation of Zn tetrahedral coordination. The bond located at 495 cm^{-1} confirmed the stretching vibration of Zn–O, indicating the metal oxygen bonding [42]. This result was consistent with the data obtained by XRD.

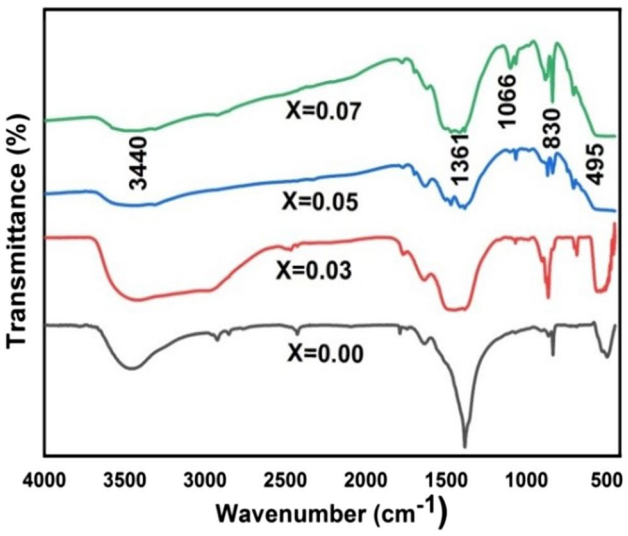

Fig. 3 FTIR spectra of $Zn_{1-x}Co_xO$ (x = 0.0, 0.03, 0.05, and 0.07) nanoparticles

XPS analysis

The chemical state and valence electron present in the material were identified by XPS measurements, as shown in Fig. 3. The surface composition of Zn, Co and O was investigated by employing the Zn2p, Co2p and O1s peaks in the XPS survey spectrum indicated in Fig. 4(a). Figure 4(b) shows the Zn2p spectrum for $Zn_{0.03}Co_{0.07}O$, which resolves doublet $Zn2p_{3/2}$ and $Zn2p_{1/2}$ centering at binding energies of 1022.5 and 1045.1 eV [43]. The spin orbital splitting energy of two peaks is 23.4 eV, which agrees well with the standard value, which confirms Zn is present as Zn^{2+} ions [44]. These two convoluted Zn2p peaks confirm the formation of hexagonal wurtzite ZnO [45]. The binding energies of $Co2p_{3/2}$ and $Co2p_{1/2}$ located at 780.24 eV and 797.02 eV, respectively, in Fig. 4(c), indicating that cobalt can substitute in the Zn cation site with the Co^{2+} oxidation state [46]. The difference in binding energies found to be 17.22 eV for Co2p ions indicates that Co ions may have a bivalent ZnO lattice with a high spin d state. The amount of cobalt ion incorporated in the sample was smaller, so the XPS peaks for Co2p were not intense. Figure 4(d) for O1s had a single peak located at 532.1 eV, which was attributed to the O^{2-} ions corresponding to the lattice oxygen of ZnO [47]. The intensity of this peak indicates that the difference may generate defects in ZnO nanoparticles and a number of oxygen vacancies. Hence, XPS analysis further confirms the prepared $Zn_{0.03}Co_{0.07}O$ nanoparticle has high purity and a single phase without the formation of secondary phases. Also, Co ions are decorated on the surface of ZnO.

HR-TEM analysis

The information about crystalline structure, size, surface morphology and shape of nanoparticles was analysed using HR-TEM images and SAED patterns. ZnO nanoparticles show a nearly spherical shape with agglomeration (Fig. 5a) [48]. Whereas, $Zn_{0.93}Co_{0.07}O$ nanoparticles are composed of hexagonal structure with an uneven grain boundary (Fig. 5d) and the obtained product was in good agreement with XRD results. Lattice fringes in the HRTEM image correspond to diffracted and transmitted waves exiting one plane of the crystal [49]. The lattice spacing of 0.24 nm and 0.26 nm in the (101) plane represents the hexagonal wurtzite structure of ZnO (Fig. 5c) and $Zn_{0.93}Co_{0.07}O$ (Fig. 5e) respectively. The concentric circle dotted with bright spots in the SAED pattern indicates the diffraction planes are due to the polycrystalline nature of the hexagonal wurtzite crystal structure.

SEM analysis

Surface morphology, size and shape of biosynthesized pure and Co doped ZnO nanoparticles have been described by

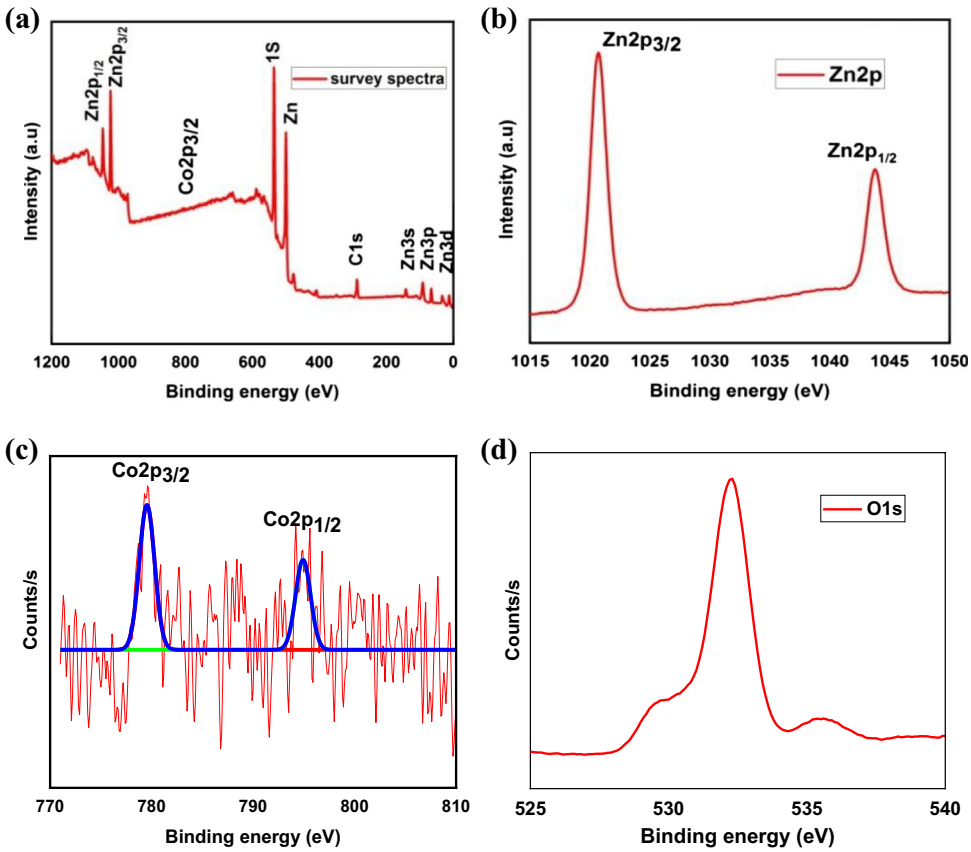

Fig. 4 XPS spectra of (**a**) $Zn_{0.03}Co_{0.07}O$ survey spectra (**b**) Zn 2p (**c**) Co 2p (**d**) O1s

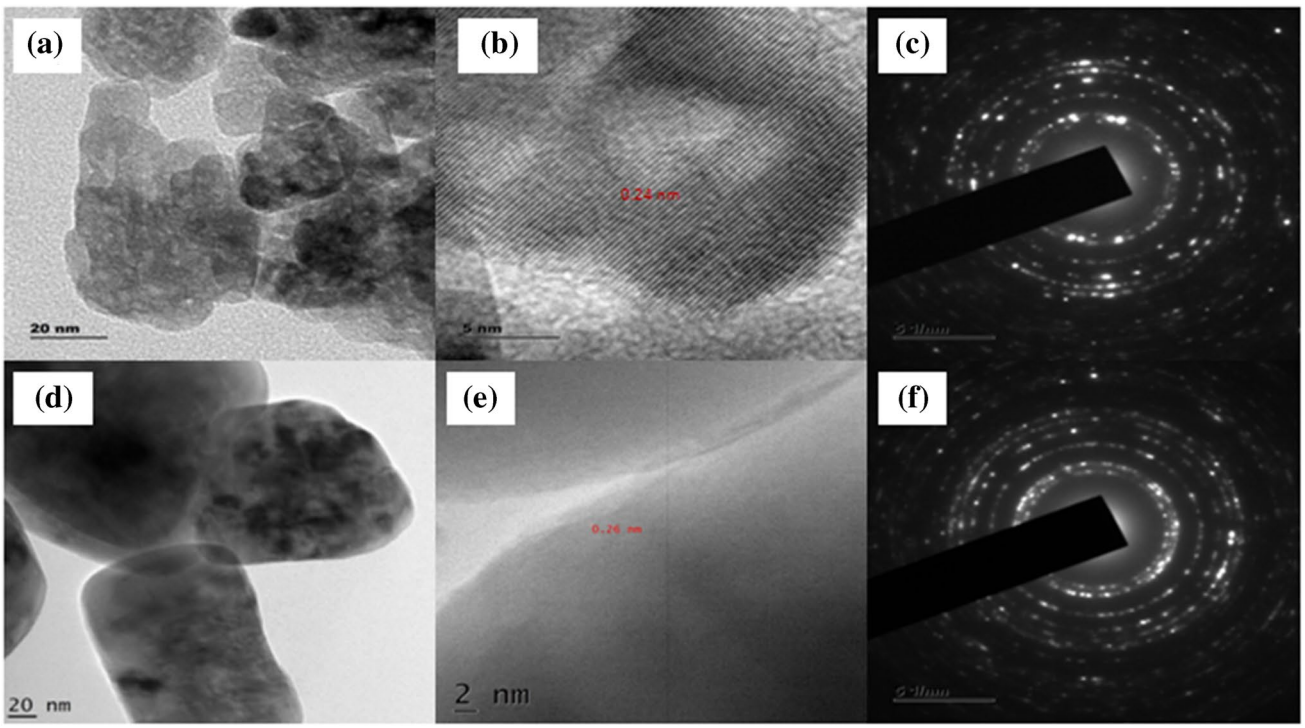

Fig. 5 HR-TEM image (**a**) ZnO (**d**) $Zn_{0.93}Co_{0.07}O$, fringe width (**c**) ZnO (**e**) $Zn_{0.93}Co_{0.07}O$, SAED pattern (**e**) ZnO, (**f**) $Zn_{0.93}Co_{0.07}O$

SEM analysis. ZnO nanoparticles are aggregated to form a cauliflower-like structure [50], as demonstrated in the micrograph of Fig. 6(a). While Co doping indicates that most nanoparticles are agglomerated due to their larger surface area (Fig. 6b). EDX spectra indicate Zn and O elements are present in pure ZnO (Fig. 6c) at the same time as the presence of Zn, Co and O in Co doped ZnO confirms the presence of Co^{2+} ions as substitutes for the Zn^{2+} ions in the ZnO matrix (Fig. 6d) [51]. Thus, it can be verified that Co-ions are successfully incorporated into the ZnO lattice without any impurities. The quantitative analysis of atomic and weight percentage was listed on inset tables in Fig. 6c, d.

UV visible analysis

Figure 7(a) displays optical absorption spectra of $Zn_{1-x}Co_xO$ (x = 0.0, 0.03, 0.05, and 0.07) nanoparticles. ZnO is a direct bandgap semiconductor and the optical bandgap can be found out by extrapolating linear portion in the plot of $(\alpha h\nu)^2$ against $h\nu$ using Tauc's relation,

$$\alpha h\nu = k(h\nu - Eg)^{1/n} \quad (14)$$

where α is the absorption coefficient, $h\nu$ is the photon energy, Eg is the bandgap energy of the material and k is

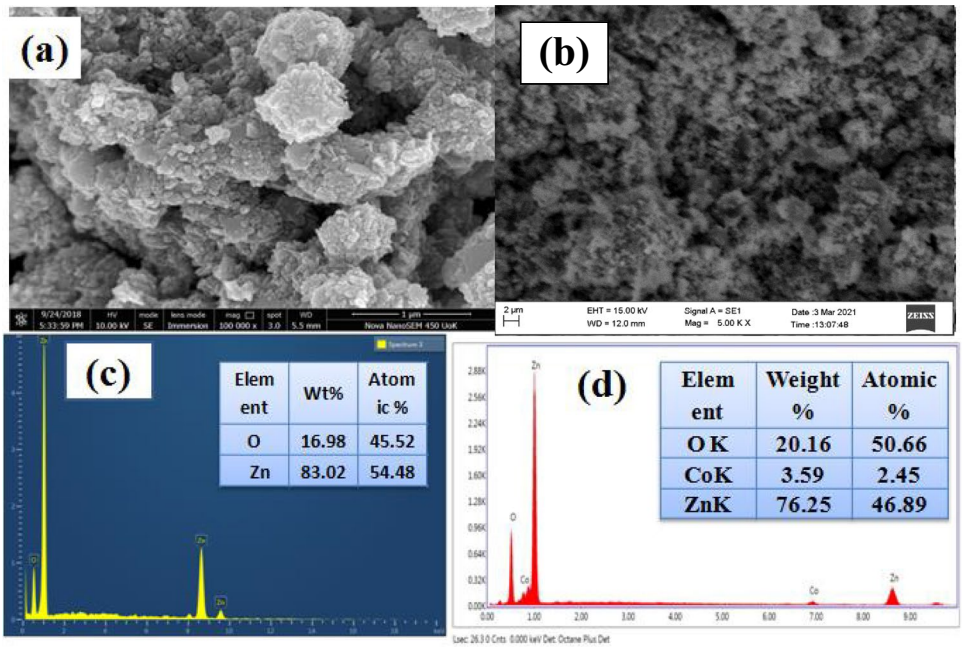

Fig. 6 SEM image (**a**) ZnO (**b**) $Zn_{0.93}Co_{0.07}O$, EDX spectra (**c**) ZnO (**d**) $Zn_{0.93}Co_{0.07}O$

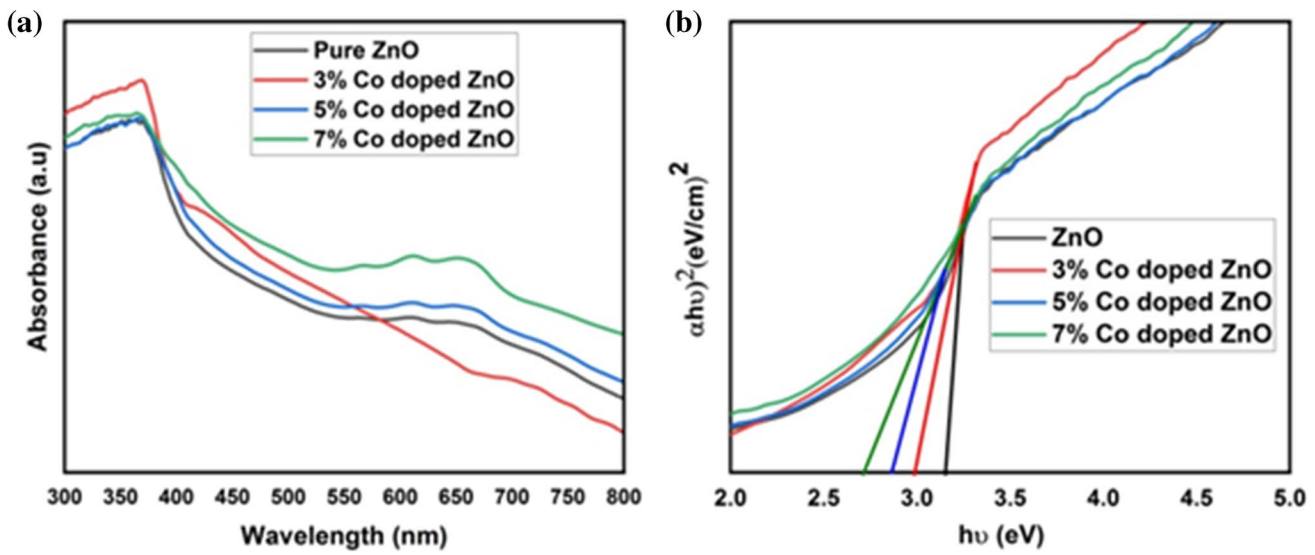

Fig. 7 UV–Visible absorption spectra of $Zn_{1-x}Co_xO$ (x = 0.0, 0.03, 0.05, and 0.07) nanoparticles

a constant. The estimated bandgap is 3.15 eV, 3.00 eV, 2.87 eV and 2.71 eV for 0%, 3%, 5% and 7% Co-doped ZnO nanoparticles respectively from Fig. 7(b).Decrease in bandgap with increase in Co concentration was occurred through increase in adsorption edge as well as the electrons in sp-d spin-exchange interaction between localized spins of transition metal ions and the localized d electron of Co^{2+} ions substituting Zn^{2+}ions [52]. The reduction in bandgap may be due to the crystallinity of nanoparticles, carrier concentration, grain size as well as s-d and p-d exchange interaction [53]. Co-doping gives structural deformation of interstitial zinc ions and it gives additional energy levels in the valance band edge of host ZnO linked to direct transition [54].

The valence band (E_{vb}) and conduction band (E_{cb}) position of semiconductor nanoparticles are estimated using Muliken electronegativity theory [55],

$$E_{vb} = \chi - E^0 + 0.5E_g \tag{15}$$

$$E_{cb} = \chi - E^0 - 0.5E_g \tag{16}$$

where χ is the absolute electronegativity of ZnO (5.79), E^0 is the constant value of free electron energy on the hydrogen scale (4.5) and E_g is the optical band gap of the material [56]. The estimated valence band and conduction band edges from direct band gap of nanoparticles are 2.865 eV, 2.79 eV, 2.725 eV, 2.645 eV, -0.285 eV, -0.21 eV, -0.145 eV, -0.065 eV respectively for 0%, 3%, 5% and 7% Co doped ZnO nanoparticles.

Refractive index is a measure of transparency of incident spectral radiation, semiconductor materials with high refractive index and wide bandgap have applications in optical interference filters, optoelectronics and sensor (anti reflection coating) industry [56]. If the band gap of a material is known, the refractive index of semiconductor can be calculated using the following models,

Moss relation,

$$n = \left(\frac{k}{E_g}\right)^{\frac{1}{4}} \tag{17}$$

where k is a constant having value 108 eV.

Vandamme's relation,

$$n = \sqrt{1 + \left(\frac{A}{Eg + B}\right)^2} \tag{18}$$

where A = 13.6 eV and B = 3.4 eV.

Liner relation proposed by Ravindra for variation of optical refractive index with energy gap between bonding and antibonding states,

$$n = 4.08 - 0.62Eg \tag{19}$$

Anani proposed an empirical relationship between refractive index (n) and bandgap (Eg) of solids as follows,

$$n = \frac{(17 - Eg)}{5} \tag{20}$$

The data for the UV edge, bandgap, refractive index, valence and conduction band edges are summarised in Table 2. The variation in bandgap with Co doping on ZnO nanoparticles may be attributed to oxygen vacancy availability, which causes transition of electrons from a valence band to a conduction band. As the concentration of oxygen vacancy increases, impurity states of ZnO become more delocalized and overlap with valance band edges, thus reducing the bandgap.

Antibacterial activity

The antibacterial activity of synthesized $Zn_{1-x}Co_xO$ (x = 0.0, 0.03, 0.05, and 0.07) nanoparticles was tested against *P.aeruginosa, S.aureus* and *B. subtilis,* as shown in Fig. 8(a-l) and the zone of inhibition is depicted in Table 3. The result shows effective antimicrobial activity against *S.aureus* has zone of inhibition of 13 mm, 12 mm, 12 mm and 13 mm for 0%, 3%, 5% and 7% cobalt doped ZnO nanoparticles at 80 µL concentration (Fig. 8a-d). *P.aeruginosa* has zone of inhibition of 11 mm, 12 mm, 12 mm and 13 mm for 0%, 3%, 5% and 7% Co-doped ZnO nanoparticles respectively at 80

Table 2 UV edge, Band gap, Refractive index, valence and conduction band edges of $Zn_{1-x}Co_xO$ (x = 0.0, 0.03, 0.05 and 0.07) nanoparticles

Sample		ZnO	$Zn_{0.97}C_{0.03}O$	$Zn_{0.95}Co_{0.05}O$	$Zn_{0.93}Co_{0.07}O$
UV edge (nm)		356	366	370	373
Band gap (eV)		3.15	3.00	2.87	2.71
Refractive index (n)	Moss	2.419793	2.44949	2.476769	2.512544
	Vandamme's	2.304598	2.348537	2.388476	2.440174
	Ravindra	2.127	2.22	2.3006	2.3998
	Anani	2.77	2.8	2.826	2.858
Valence Band Edge (E_{vb})(eV)		2.86	2.79	2.725	2.645
Conduction Band Edge (E_{cb})(eV)		-0.29	-0.21	-0.145	-0.065

µL concentrations (Fig. 8e-h). *B.subtilis* has zone of inhibition of 12 mm, 11 mm and 14 mm for 0%, 5% and 7% of cobalt doped ZnO nanoparticles at sample concentration 80 µL (Fig. 8i-l). *P.aeruginosa* has higher antibacterial activity compared to *B.subtilis* and *S.aureus* because of the thinner and impermeable peptidoglycan layer of gram-negative bacteria. Higher concentrations of cobalt doping have a higher bactericidal potential than the standard drug Gentamycin due to their lower toxicity, grain size, shape, and surface area [57]. This allows increase in biological activity in everyday life applications such as sports cloths, medical textiles and bed clothes [58].

The greater antibacterial activity was due to the fact that when Co-ZnO nanoparticles enter the cell wall of bacteria, they produce electrostatic interaction between the negatively charged outer surface of bacteria and positively charged Zn^{2+}, Co^{2+} ions via, uptake of metal ions into the cells [59].So, metal ions produces induced oxidative stress and reactive oxygen species which damages the cellular structure, DNA, lipopolysaccharides, proteins, bacterial membrane permeability, intercellular factors, and enzymes [60]. These leads to bacterial cell death [61]. Also antibacterial activity of Co doping may be increased by the decreasing bandgap due to the doping of Co ion into the ZnO lattice which generate higher reactive oxygen species [62]. The schematic diagram for antimicrobial action was represented in Fig. 9. ZnO is highly biocompatible with human cells, low toxicity, no irritation to eye and skin so it is used for therapeutic purpose as creams, ointments to prevent sun burn and other skin care products [63]. Production of textile material with ZnO coating is useful for self-cleaning purposes via creation of hydrophilic surfaces by photocatalytic activity and antimicrobial protection. *S.aureus* bacteria cause infectious diseases in athletic teams. So antibacterial sports clothing, which prevents microbial growth and sweat odour during sports activity, revolutionized the sportswear market [64].

Antifungal activity

The antifungal activity of 0%, 3%, 5% and 7% Co doped ZnO nanoparticles against *Candida Albicans* and *Aspergillus*

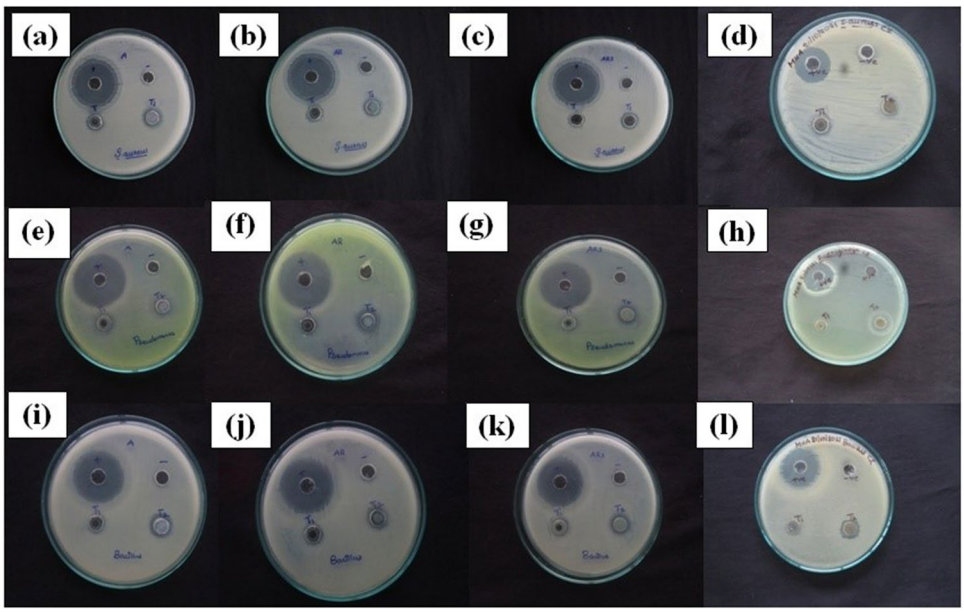

Fig. 8 Antibacterial activity of $Zn_{1-x}Co_xO$ nanoparticles against *Staphylococcus aureus* (**a**) x = 0, (**b**) 0.03, (**c**) 0.05 (**d**) 0.07, *Pseudomonas aeruginosa* (**e**) x = 0, (**f**) 0.03, (**g**) 0.05 (**h**) 0.07, *Bacillus subtilis* (**j**) x = 0, (**j**) 0.03, (**k**) 0.05 (**l**) 0.07 Co doping concentration

Table 3 Antibacterial activity of $Zn_{1-x}Co_xO$ (x = 0, 0.03, 0.05 & 0.07) nanoparticles for *Staphylococcus aureus, Pseudomonas aeruginosa* and *Bacillus subtilis*

Nanoparticles	Zone of inhibition								
Organisms	*Staphylococcus aureus*			*Pseudomonas aeruginosa*			*Bacillus subtilis*		
Concentration	T1	T2	Gentamycin (160 mcg)	T1	T2	Gentamycin (160 mcg)	T1	T2	Gentamycin (160 mcg)
ZnO	11	13	26	-	11	28	-	12	27
$Zn_{0.97}Co_{0.03}O$	11	12	26	-	12	28	-	-	21
$Zn_{0.95}Co_{0.05}O$	-	12	26	-	12	30	-	11	25
$Zn_{0.93}Co_{0.07}O$	-	13	24	11	13	22	-	14	27

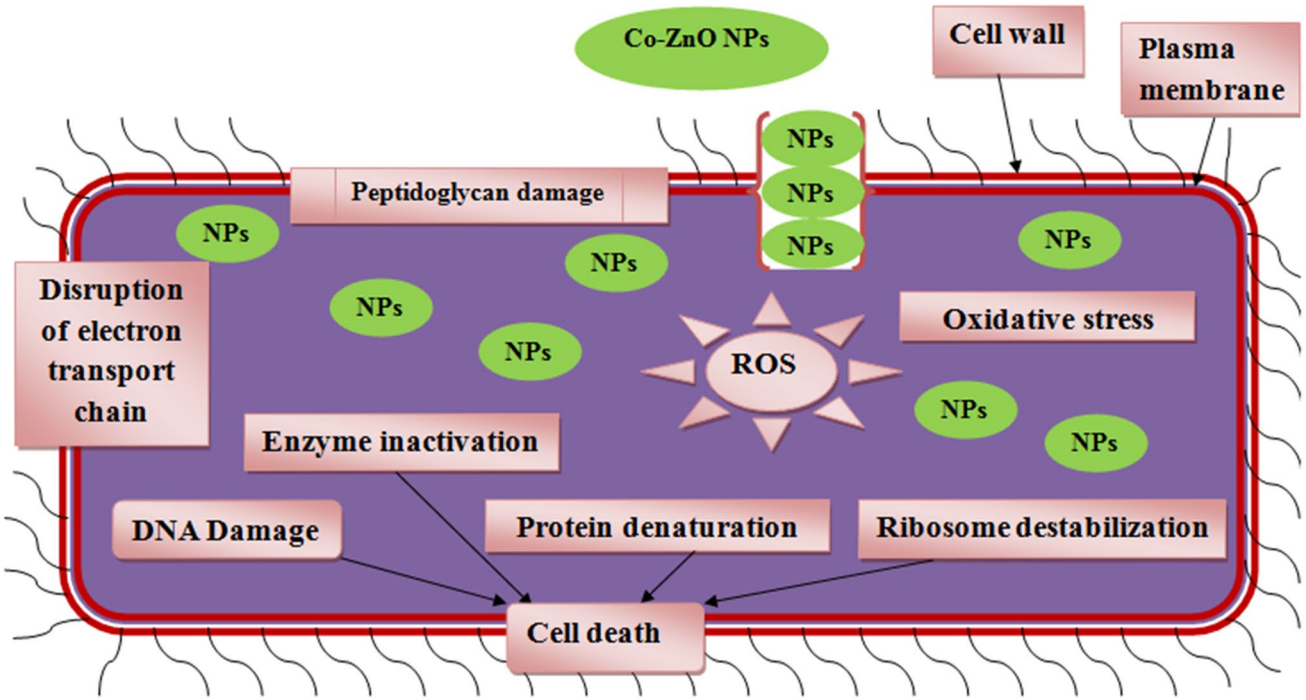

Fig. 9 antimicrobial mechanism of nanoparticles against microbial cells

niger was shown in Fig. 10, and the zone of inhibition was represented in Table 4. 0%, 3%, 5% and 7% Co doped ZnO nanoparticles showed significant antifungal activity against *Candida Albicans* with zone of inhibition of 16 mm, 20 mm, 15 mm and 22 mm with 1000 µg concentration respectively. *Aspergillus niger* shows zones of inhibition of 15 mm, 13 mm, 12 mm and 16 mm for 0%, 3%, 5% and 7% Co doped ZnO nanoparticles. The antifungal activity of nanopowder was compared with that of the standard drug clotrimazole, and the antifungal potential was observed more in *Candida Albicans* than in *Aspergillus niger*. The higher antifungal activity for the higher doping level of Co may be due to an increase in crystallite size and a decrease in bandgap [65]. As a result, Co doped ZnO nanoparticles exhibit a broad range of antifungal activities.

Reactive oxygen species formed from ZnO nanoparticles damage the DNA and cause denaturation of proteins. The ionic interaction of ZnO nanoparticles on the cell wall leads to the death of cell wall (Fig. 9). Some reports suggest that the discharge of lipids, nucleic acids and proteins alters the membrane permeability of fungal cells, but the high content of carbohydrate creates self-protecting mechanism against nanoparticles. According to these findings, ZnO nanoparticles can inhibit the lipid and protein content in the cell

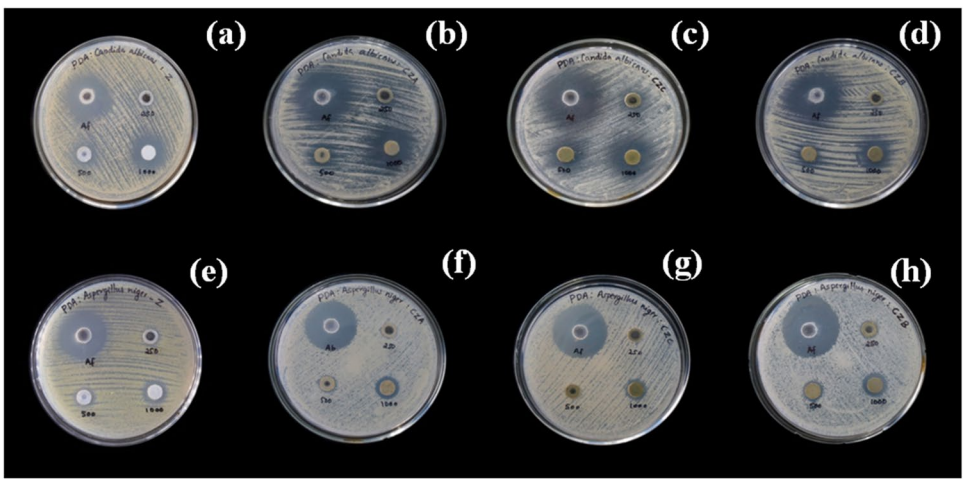

Fig. 10 Antifungal activity of $Zn_{1-x}Co_xO$ nanoparticles for *C. albicans* (**a**) x = 0, (**b**) 0.03, (**c**) 0.05 (**d**) 0.07 nanoparticles, ***A. niger*** (**e**) x = 0, (**f**) 0.03, (**g**) 0.05 (h) 0.07 07 nanoparticles

Table 4 Antifungal activity of $Zn_{1-x}Co_xO$ (x = 0.0, 0.03, 0.05 and 0.07) nanoparticles against *Candida albicans* and *Aspergillus niger*

Nanoparticles	Zone of inhibition(mm)							
	Candida albicans				*Aspergillus niger*			
Concentration(µg)	**250**	500	1000	**Clotrimazole 100 µg**	250	500	1000	**Clotrimazole 100 µg**
ZnO	NA	12	16	27	11	13	15	29
$Zn_{0.97}Co_{0.03}O$	12	14	20	30	NA	11	13	30
$Zn_{0.95}Co_{0.05}O$	NA	13	15	30	NA	NA	12	30
$Zn_{0.93}Co_{0.07}O$	13	15	22	30	11	12	16	30

membrane, while increasing carbohydrate content in the cell membrane results in antifungal activity [49].

Antioxidant activity

Antioxidant activity was measured by neutralising free radicals that are able to respond to various life-threatening diseases by donating an electron. Antioxidants are capable of scavenging or inhibiting the production of reactive oxygen species [66]. The phytochemical constituent of polyphenols reveals significant antioxidant activity due to absorption and neutralization of free radicals, quenching of singlet and triplet oxygen, as well as flavonoids capped on the surface of nanoparticles, which have increased antioxidant activity of nanoparticles [67]. The colour change of DPPH with the reduction by nanoparticles from purple to yellow was confirmed by the decreasing in absorbent value at 517 nm [68]. The antioxidant activity of nanoparticles increases with increasing concentration. The IC50 value was depicted for expressing 50% of inhibition and the obtained IC50 values for ZnO and $Zn_{0.93}Co_{0.07}O$ nanoparticles are 252.187 µg/mL and the 150.665 µg/mL respectively (Fig. 11). Many reports suggest that metal and metal oxide nanoparticles exhibit better antioxidant properties.

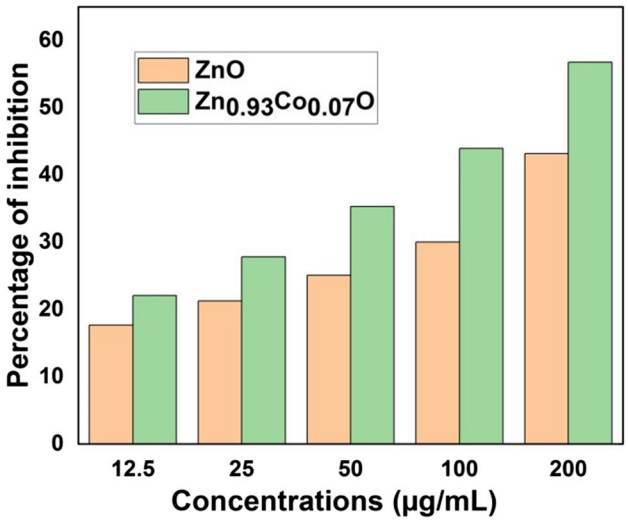

Fig. 11 Antioxidant activities of ZnO and $Zn_{0.93}Co_{0.07}O$

Cytotoxicity assay

ZnO has received considerable attention in the field of nanotechnology due to its cosmetics, sports industry and biomedical applications. On the increasing sample dosage, the green synthesised ZnO nanoparticles represent enhanced cell viability of L929 normal fibroblast cell lines, represented in Fig. 12, and the phase contrast microscopic images are shown in Fig. 13. The obtained LD50 value of ZnO nanoparticle is 5.9569 µg/µl. The cytotoxicity of cells and tissues depends on several factors, including size distribution, morphology, surface chemistry, surface charge, shape, capping agents, cell type etc. Factors such as induction of membrane leakage, DNA fragmentation and ability to activate the apoptotic mechanism by the generation of ROS may be due to the toxic effects of nanoparticles. The obtained phase contrast images confirm the damage of cell morphology was related to dose concentration of ZnO nanoparticles, and the decreased in viability of cancer cells suggest oxidative stress caused by nanoparticles resulted in cell death.

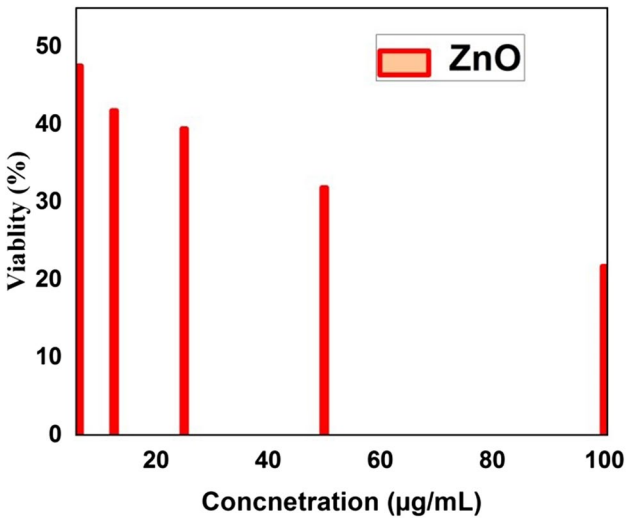

Fig. 12 Percentage viability versus concentration of ZnO nanoparticles against L929 fibroblast

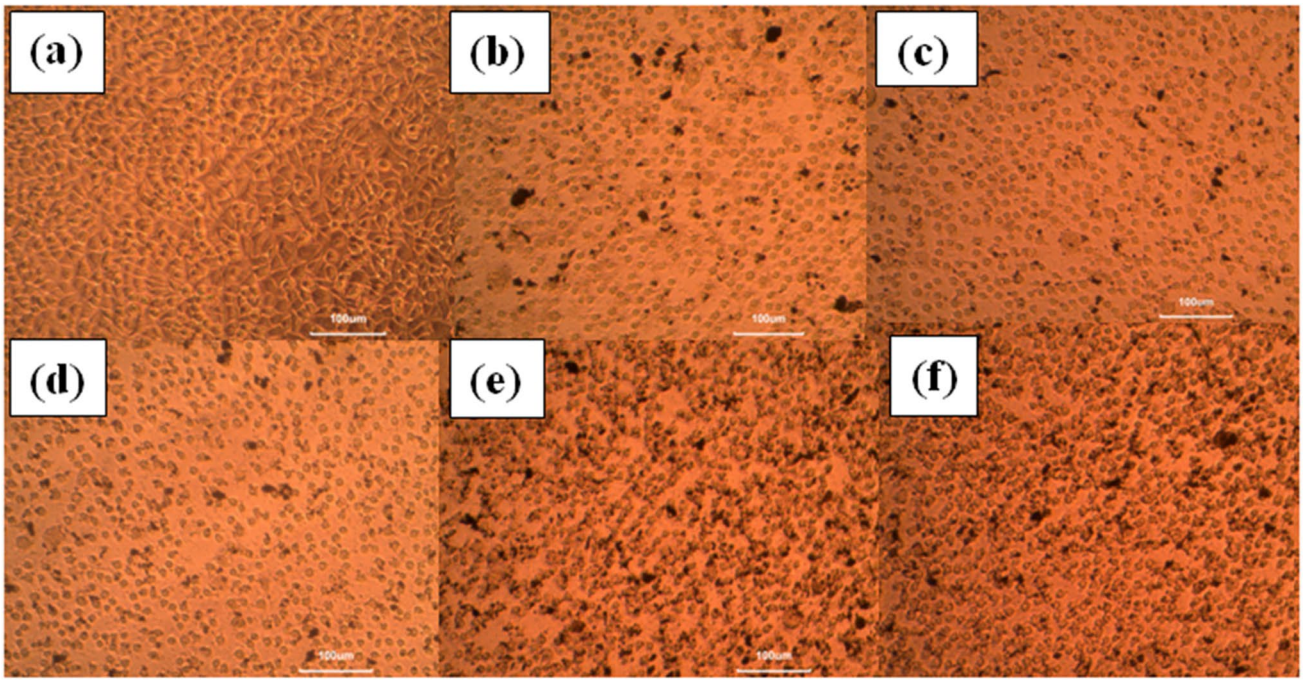

Fig. 13 Microscopic images of cell treated with various concentration of CuO nanoparticles (**a**) control (**b**) 6.25 (µg/mL), (**c**) 12.5 (µg/mL), (**d**) 25 (µg/mL), (**e**) 50 (µg/mL), (**f**) 100 (µg/mL)

Photocatalytic study

The photocatalytic performances of ZnO and $Zn_{0.93}Co_{0.07}O$ catalyst were investigated for the degradation of MB under sunlight irradiation. The UV–Visible spectrometer was used to measure the absorbance of the mixture, and the percentage of dye degradation was calculated from the expression [69],

$$Degradation\ efficiency, \% = \frac{C_0 - C_t}{C_0} \times 100 \tag{21}$$

where C_0 and C_t are the dye absorbance before degradation and final absorbance of dye at different time intervals "t" of sunlight irradiation. The reaction rate constant of dye degradation was calculated by using pseudo-first order kinetic equation,

$$C_t = C_0 e^{-kt} \tag{22}$$

$$\ln\left(\frac{C_t}{C_0}\right) = -kt \tag{23}$$

Here k is the first order rate constant (min^{-1}) and t is the photo-irradiation time (min). The slope of the linear fitted curve of $\ln\left(\frac{C_t}{C_0}\right)$ vs. time gives the value of rate constant k.

In this work, ZnO and $Zn_{0.93}Co_{0.07}O$ nanoparticles are used as photocatalysts and MB solution is used as a target pollutant. The degradation of MB was confirmed by a high intensity peak at 660 nm; this peak decreased rapidly with an increase of degradation time, and no new peaks appeared during the reaction. The time-dependent absorption spectra of ZnO and $Zn_{0.93}Co_{0.07}O$ nanoparticles were shown in Fig. 14 (a, b), respectively. Approximately 92% and 95% of MB was degraded in 120 min, suggesting the complete degradation of photocatalyst for ZnO and $Zn_{0.93}Co_{0.07}O$ nanoparticles as indicated in Fig. 14 (c). The kinetics of degradation reaction were determined from a pseudo first order kinetic model, as discussed in a previous report [70]. Figure 14 (d) shows that it obeys pseudo first order kinetics, which states that as time increases, C/C_0 decreases[71]. Also, the graph shows a linear relationship with a high correlation coefficient (R^2) indicating that methylene blue degradation by the prepared photocatalysts follows pseudo first order kinetics under sunlight irradiation [72], which confirms that the suggested model is valid [73]. The obtained rate constant values are 0.02053 min^{-1} and 0.02252 min^{-1} and the obtained R^2 values are 0.88074 and 0.92238 for ZnO and $Zn_{0.93}Co_{0.07}O$ nanocatalysts, respectively. Therefore, the ZnO and $Zn_{0.93}Co_{0.07}O$ nanoparticles show good photocatalytic activity with regards to degradation of MB and act as catalysts. The enhancement in catalytic performance of $Zn_{0.93}Co_{0.07}O$ nanoparticles is due to a decrease in bandgap and compared with the photodegradation efficiency of other synthesised ZnO nanoparticles listed in Table 5. Surface oxygen vacancies present in the nanoparticles increase the electron–hole pairs, which increase adsorption of oxygen

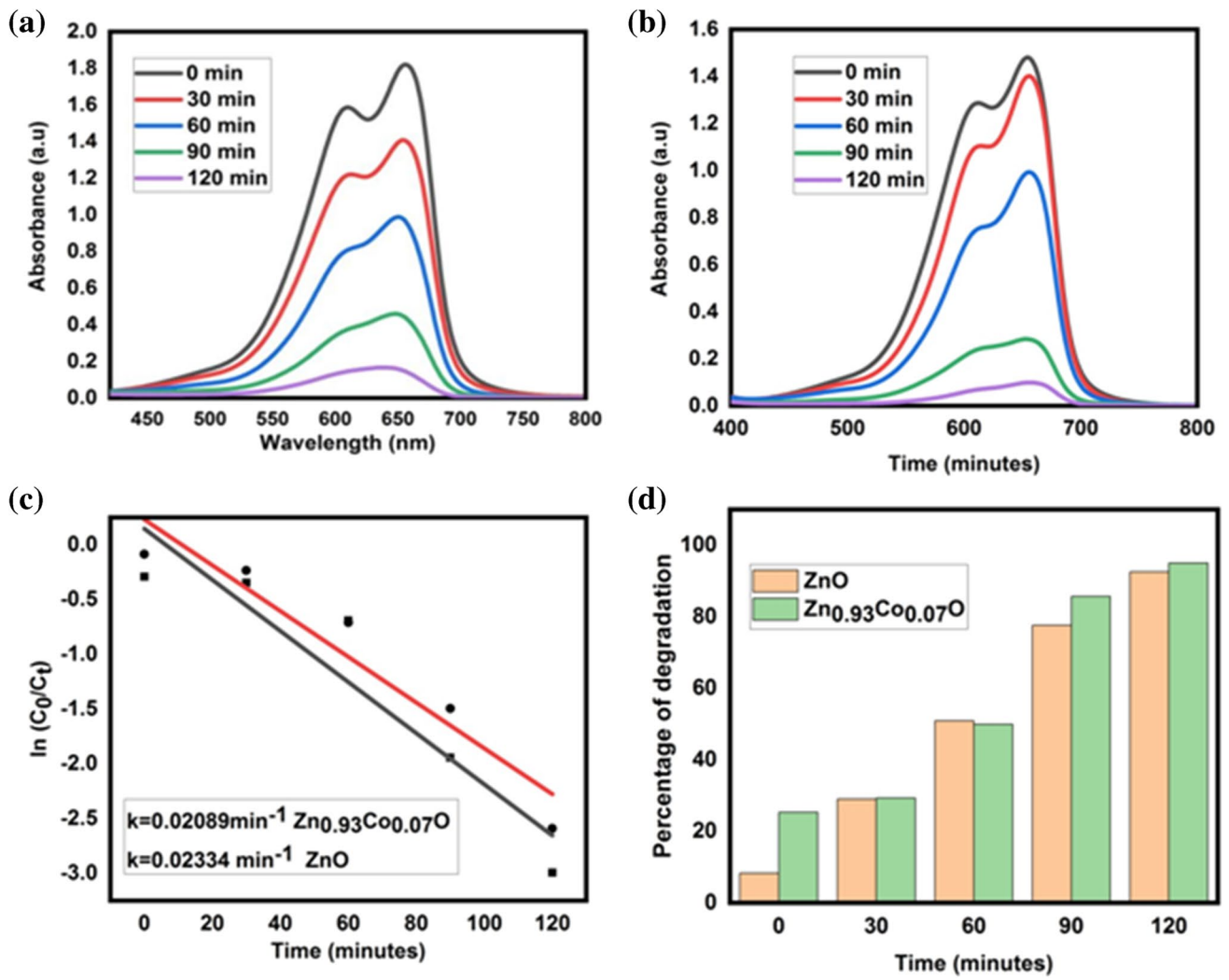

Fig. 14 MB Time dependent absorption spectra (**a**) ZnO, (**b**) $Zn_{0.93}Co_{0.07}O$, (**c**) percentage of dye degradation, (**d**) kinetic study of ZnO, $Zn_{0.93}Co_{0.07}O$

and create oxygen vacancies, which produce energy levels within the band gap of the nanoparticles. The energy levels trap the charge carriers and capture the photogenerated charges, delaying electron–hole pair recombination. These trapped carriers enhance the formation of active species that enhance photocatalytic activity. Also, oxygen vacancies help the adsorption of oxygen on the ZnO surface, leading to the generation of superoxide radicals. As a result, photocatalytic performance increases [74].

Photocatalytic mechanism

The photocatalysis mechanism for Co doped ZnO nanoparticles has been illustrated in Fig. 15. ZnO is an n-type semiconductor material with a wide bandgap. The calculated direct band gap based on UV–Visible absorption spectra was 3.15 eV and 2.17 eV for ZnO and $Zn_{0.93}Co_{0.07}O$ nanoparticles, respectively. The valence and conduction band edges are calculated from Eqs. (15) and (16). Under sunlight irradiation, the electrons from the valance band get excited to the conduction band of ZnO, leaving holes in valence band that lead to the formation of electron hole pairs. Co doping results the formation of electron trap levels between the valance band and conduction band. These trap levels effectively shifted the band edge threshold [75].

$$ZnO + h\nu \rightarrow e^{-}_{CB} + h^{+}_{VB} \tag{24}$$

The photogenerated electron and hole pairs migrate on the surface of nanoparticles, producing a redox reaction. This leads to the generation of highly active hydroxyl radicals, which are responsible for the degradation of organic dyes. The oxygen vacancy defects (singly ionized oxygen,

Table 5 Comparison of photocatalytic efficiency of biosynthesised ZnO nanoparticles with recently reported work

sample	Synthesis method	Energy source	Irradiation time(min)	Degradation efficiency	Reference
ZnO	Green synthesis	Visible light	90	83.45%	[74]
ZnO	Green synthesis	UV light	90	88.37%	[75]
ZnO	Green synthesis	UV light	120	83%	[76]
ZnO	Green synthesis	UV light	150	97%	[77]
ZnO	Green synthesis	Sunlight	180	91.4%	[78]
ZnMnO	Green synthesis	Sunlight	120	95%	[19]
ZnO	Green synthesis	Sunlight	120	92%	Present work
ZnCoO	Green synthesis	Sunlight	120	95%	Present work

doubly charged state) and doped Co on the surface of ZnO improve electron–hole pair separation [76]. The released electron from the conduction band reacts with molecular oxygen (acceptor), forming a super oxide anion [77].

$$e_{CB}^{-} + V_0^{++} \rightarrow V_0^{+} \tag{25}$$

$$O_2 + V_0^{+} \rightarrow V_0^{++} + O_2^{-} \tag{26}$$

$$Co \rightarrow Co^{2+} + 2e^{-} \text{ or } e_{CB}^{-} \tag{27}$$

$$e^{-} \text{ or } e_{CB}^{-} + O_2 \rightarrow O_2^{-}(\text{Super Oxide Anion}) \tag{28}$$

Co takes electrons from conduction band of ZnO and decreases the electron hole pair recombination probability and makes more holes available for OH^- radical formation

$$2e_{CB}^{-} + Co^{2+} \rightarrow Co \tag{29}$$

The holes from valence band react with (OH^-) moisture in air forming hydroxyl radical (OH^-) and H_2O forming (OH^-) radical H^+ ions [78].

$$h_{VB}^{+} + OH^{-} \rightarrow OH^{-} + H^{+} \tag{30}$$

$$h_{VB}^{+} + H_2O \rightarrow OH^{-} \tag{31}$$

The generated O^- radical oxidize water H_2O forms H_2O_2, this further reacts with electrons forms OH^- radicals [19].

$$O_2^{-} + H_2O \rightarrow H_2O_2 \tag{32}$$

$$H_2O_2 + e_{CB}^{-} \rightarrow 2OH^{-} \tag{33}$$

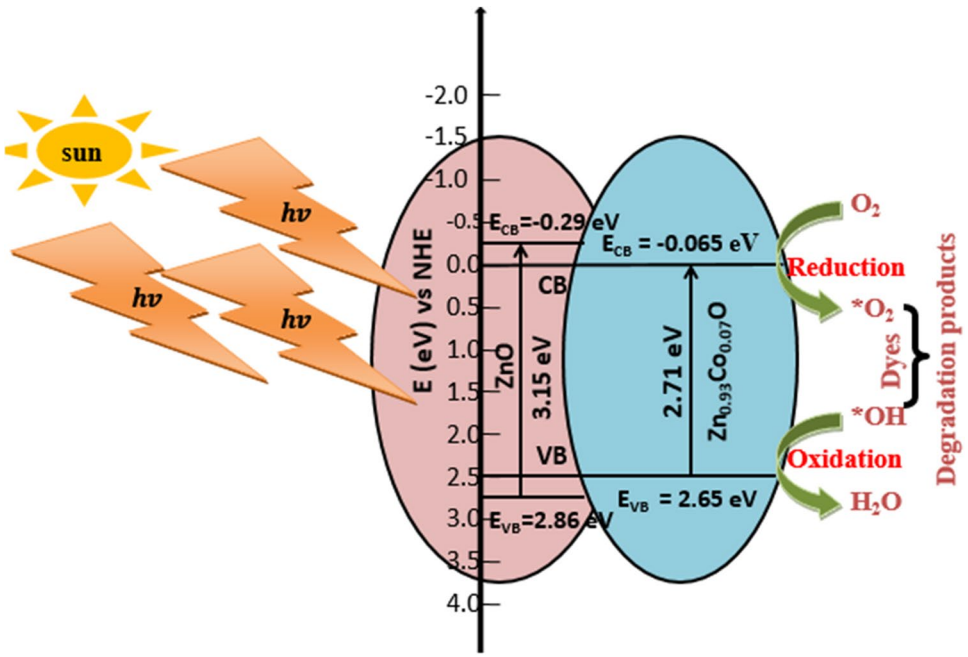

Fig. 15 Simple mechanism to understand photocatalytic degradation under solar light

The formed O_2^- and OH^- undergo oxidative reaction with pollutants forming H_2O and Co_2 and less toxic materials [79].

$$\text{Organic dyes} + O_2^- + OH^- \rightarrow H_2O + CO_2 + \text{Less toxic materials} \quad (34)$$

Therefore, the presence of Co^{2+} in ZnO affects the charge transfer kinetics and separation of photogenerated e^-/h^+ pairs, resulting in enhanced photocatalytic degradation of MB. The superoxide anion and hydroxyl radicals break down organic compounds and oxidize MB dyes into minerals as end product [80]. The results of photocatalytic degradation show green synthesized ZnO and $Zn_{0.93}Co_{0.07}O$ act as potential catalysts for the degradation of commercial dyes.

Conclusion

In this work, we have synthesized 0%, 3%, 5% and 7% Co doped ZnO nanoparticles by the green method for photocatalytic degradation of MB and its biological activities. The XRD pattern confirms the formation of the hexagonal wurtzite structure of ZnO, and the FTIR spectra assures the formation of Zn–O. Morphology of nanoparticles identified by SEM and HR-TEM analysis. EDX evident the presence of Co dopants along with Zn and O. UV–Visible absorption spectra has decrease in energy by Co doping. The ZnO and $Zn_{0.93}Co_{0.07}O$ nanoparticles show photocatalytic degradation efficiencies of 92% and 95% under sunlight irradiation for MB within 120 min. Based on the antimicrobial analysis, it can be concluded that as the concentration of Co^{2+} increases, $Zn_{0.93}Co_{0.07}O$ nanoparticles can effectively destroy various disease-causing bacteria, which indicates strong antimicrobial activity. Also, the nanoparticle shows good antioxidant and cytotoxicity activities. Thus, the obtained result demonstrates a simple, cost-effective, bio-compatible, eco-friendly green method can be used for the synthesis of pure and Co doped ZnO nanoparticles using *Annona Muricata* leaf extract and has potential applications in environmental and biomedical fields.

Acknowledgements Vindhya P S like to thank University of Kerala for financial support under university Junior Research Fellowship. Authors thanks CLIF Kerala University, DST-SAIF Cochin for characterization studies and BIOGENIX research centre, Thiruvananthapuram for antimicrobial, antioxidant, and cytotoxicity studies.

Authors contribution Vindhya P S, Kavitha V T concept and design of the work. Vindhya P S designed the experiments, synthesized, characterized and their applications were done on the material. Vindhya P S, Sandhya Suresh, Kunjikannan R and Kavitha V T analysed the data. All authors discussed the results of the manuscript and approved the final manuscript.

Availability of data and materials The data that support the findings of this study are available upon reasonable request from the authors.

Declarations

Ethics approval and consent to participate Not applicable.

Consent for publication Not applicable.

Conflict of interest The authors declare that they have no competing interests.

References

1. Rani H, Prakash S, Prasad T, Sajid M, Israil M, Kumar A. In-vitro catalytic, antimicrobial and antioxidant activities of bioengineered copper quantum dots using Mangifera indica (L.) leaf extract. Mater Chem Phys. 2020;239:122052. https://doi.org/10.1016/j.matchemphys.2019.122052.
2. Ullah I, Tahir K, Ullah A, Albalawi K, Li B. Facile fabrication of Ag nanoparticles: An advanced material for antioxidant, infectious therapy and photocatalytic applications Facile fabrication of Ag nanoparticles: An advanced material for antioxidant , infectious therapy and photocatalytic applications. Inorg Chem Commun. 2022;141:109539. https://doi.org/10.1016/j.inoche.2022.109539.
3. Ahmad B, Khan MI, Naeem MA, Alhodaib A, Fatima M, Amami M, et al. Green synthesis of NiO nanoparticles using Aloe vera gel extract and evaluation of antimicrobial activity. Mater Chem Phys. 2022;288:126363. https://doi.org/10.1016/j.matchemphys.2022.126363.
4. Zhang L, Ding Y, Povey M, York D. ZnO nanofluids – A potential antibacterial agent. Prog Nat Sci. 2008;18:939–44.
5. Nazir A, Akbar A, Baghdadi HB, Rehman S, Al-Abbad E, Fatima M, et al. Zinc oxide nanoparticles fabrication using Eriobotrya japonica leaves extract: Photocatalytic performance and antibacterial activity evaluation. Arab J Chem. 2021;14:103251. https://doi.org/10.1016/j.arabjc.2021.103251.
6. Zaman QU, Anwar S, Mehmood F, Nawaz R, Masood N, Nazir A, et al. Experimental modeling, optimization and comparison of coagulants for removal of metallic pollutants from wastewater. Zeitschrift fur Phys Chemie. 2021;235:1041–53.
7. Bokhari TH, Mustafa G, Ahmed N, Usman M, Akram N, Ul Haq A, et al. Degradation of a pigment red 238 using UV, UV/H_2O_2, UV/H_2O_2/SnO_2 and Fenton processes. Polish J Environ Stud. 2022;31:619–23.
8. Nadeem MS, Munawar T, Mukhtar F, Naveed ur Rahman M, Riaz M, Iqbal F. Enhancement in the photocatalytic and antimicrobial properties of ZnO nanoparticles by structural variations and energy bandgap tuning through Fe and Co co-doping. Ceram Int. 2021;47:11109–21. https://doi.org/10.1016/j.ceramint.2020.12.234.
9. Bukhari A, Atta M, Nazir A, Anees-Ur-Rahman, Shahab MR, Kanwal Q, et al. Catalytic degradation of MO and MB dyes under solar and UV light irradiation using ZnO fabricated using Syzygium Cumini leaf extract. Zeitschrift fur Phys Chemie. 2022;236:659–71.
10. Iqbal M, Shar GA, Ibrahim SM, Iftikhar S, Asif M, Khan MI, et al. Synthesis and characterization of heterostructured nanoparticle for efficient photocatalytic performance for dye degradation. Zeitschrift fur Phys Chemie. 2021;235:1209–26.
11. Noreen S, Zafar S, Bibi I, Amami M, Raza MAS, Alshammari FH, et al. ZnO, Al/ZnO and W/Ag/ZnO nanocomposite and their comparative photocatalytic and adsorptive removal for

Turquoise Blue Dye. Ceram Int. 2022;48:12170–83. https://doi.org/10.1016/j.ceramint.2022.01.078.
12. Isa EDM, Shameli K, Jusoh NWC, Hazan R. Rapid photodecolorization of methyl orange and rhodamine B using zinc oxide nanoparticles mediated by pullulan at different calcination conditions. J Nanostructure Chem. 2021;11:187–202. https://doi.org/10.1007/s40097-020-00358-6.
13. Sharwani AA, Narayanan KB, Khan ME, Han SS. Photocatalytic degradation activity of goji berry extract synthesized silver-loaded mesoporous zinc oxide (Ag@ZnO) nanocomposites under simulated solar light irradiation. Sci Rep. 2022;12:1–18. https://doi.org/10.1038/s41598-022-14117-w.
14. Supriya S, Prerna DI, Santhiya P, Kannan M, Riyaz SUM. Solid state synthesis, characterization of gold nanoparticles-thymoquinone and its molecular docking studies against virulent M. Tuberculosis H37Rv strain protein and WSSV envelope protein VP28. Mater Sci Eng B. 2023;288:116187. https://doi.org/10.1016/j.mseb.2022.116187.
15. Iqbal DN, Ehtisham-ul-Haque S, Ahmad S, Arif K, Hussain EA, Iqbal M, et al. Enhanced antibacterial activity of chitosan, guar gum and polyvinyl alcohol blend matrix loaded with amoxicillin and doxycycline hyclate drugs. Arab J Chem. 2021;14:103156. https://doi.org/10.1016/j.arabjc.2021.103156.
16. Al-Dhabi NA, Arasu MV. Environmentally-friendly green approach for the production of zinc oxide nanoparticles and their anti-fungal, ovicidal, and larvicidal properties. Nanomaterials. 2018;8:279.
17. Verbic A, Gorjanc M, Simoncic B. Zinc oxide for functional textile coatings: recent advances. Coatings. 2019;550:17–23.
18. Throne-Holst H, Randles S, Greiffenhagen C, Strandbakken P, Stø E. Risk, Responsibility, Rights, Regulation and Representation in the Value Chain of Nano-products. Technoscience Prog Manag Uncertain Nanotechnol. IOS Press; 2009;31–52. https://ebooks.iospress.nl/doi/10.3233/978-1-60750-022-3-31.
19. Vindhya PS, Kunjikannan R, Kavitha VT. Photocatalytic and antimicrobial activities of pure and Mn doped ZnO nanoparticles synthesised by Annona Muricata leaf extract. Int J Environ Anal Chem. 2022;1–16. https://doi.org/10.1080/03067319.2022.2118581.
20. Türkyılmaz ŞŞ, Güy N, Özacar M. Photocatalytic efficiencies of Ni, Mn, Fe and Ag doped ZnO nanostructures synthesized by hydrothermal method: The synergistic/antagonistic effect between ZnO and metals. J Photochem Photobiol A Chem. 2017;341:39–50.
21. Gao Q, Dai Y, Li X, Yang L, Cui C, Li C. Effects of Mn dopant on tuning carrier concentration in Mn doped ZnO nanoparticles synthesized by co-precipitation technique. J Mater Sci Mater Electron. 2018;29:3568–75. https://doi.org/10.1007/s10854-017-8286-3.
22. Zelekew OA, Aragaw SG, Sabir FK, Andoshe DM, Duma AD, Kuo DH, Chen X, Desissa TD, Tesfamariam BB, Feyisa GB, Abdullah H. Green synthesis of Co-doped ZnO via the accumulation of cobalt ionontoEichhornia crassipesplant tissue and the photocatalyticdegradation efficiency under visible light. Mater Res Express. 2021;8(2): 025010.
23. Lee HJ, Kim JH, Park SS, Hong SS, Lee GD. Degradation kinetics for photocatalytic reaction of methyl orange over Al-doped ZnO nanoparticles. J Ind Eng Chem. 2015;25:199–206.
24. Reddy IN, Reddy CV, Shim J, BhAkkinepally M, Cho K Yoo, Kim D. Excellent visible-light driven photocatalyst of (Al, Ni) co-doped ZnO structures for organic dye degradation. Catal Today. 2020;340:277–85. https://doi.org/10.1016/j.cattod.2018.07.030.
25. Dhanalakshmi A, Natarajan B, Ramadas V, Palanimurugan A, Thanikaikarasan S. Structural, morphological, optical and antibacterial activity of rod-shaped zinc oxide and manganese-doped zinc oxide nanoparticles. Pramana - J Phys. 2016;87:1–9.
26. Vindhya PS, Jeyasingh T, Kavitha VT. Dielectric properties of copper oxide nanoparticles using AnnonaMuricata leaf. AIP Conference proceedings. 2019; 2162: 020021. http://aip.scitation.org/doi/abs/10.1063/1.5130231
27. Gunalan S, Sivaraj R, Rajendran V. Green synthesized ZnO nanoparticles against bacterial and fungal pathogens. Prog Nat Sci Mater Int. 2012;22(6):693–700.
28. Ali F, Hamza M, Iqbal M, Basha B, Alwadai N, Nazir A. State-of-art of silver and gold nanoparticles synthesis routes, characterization and applications: A review. Zeitschrift fur Phys Chemie. 2022;236:291–326.
29. Coria-Téllez AV, Montalvo-Gónzalez E, Yahia EM, Obledo-Vázquez EN. Annona muricata: A comprehensive review on its traditional medicinal uses, phytochemicals, pharmacological activities, mechanisms of action and toxicity. Arab J Chem. 2018;11:662–91.
30. Vindhya PS, Kunjikannan R, Kavitha VT. Bio-fabrication of Ni doped ZnO nanoparticles using *Annona Muricata* leaf extract and investigations of their antimicrobial, antioxidant and photocatalytic activities. Phys Scr. 2022;98:015830 https://iopscience.iop.org/article/10.1088/1402-4896/acaa10.
31. Singh NK, Koutu V, Malik MM. Enhancement of room temperature ferromagnetic behavior of Co-doped ZnO nanoparticles synthesized via sol–gel technique. J Sol-Gel Sci Technol. 2019;91:324–34. https://doi.org/10.1007/s10971-019-05004-4.
32. Djerdj I, Jagličić Z, Arčon D, Niederberger M. Co-doped ZnO nanoparticles: mini review. Nano scale. 2010;2(7):1096–104.
33. Godavarti U, Mote VD, Dasari M. Role of cobalt doping on the electrical conductivity of ZnO nanoparticles. J Asian Ceram Soc. 2017;5:391–6. https://doi.org/10.1016/j.jascer.2017.08.002.
34. Ahmed F, Kumar S, Arshi N, Anwar MSS, Koo BH, Lee CG. Doping effects of Co2+ ions on structural and magnetic properties of ZnO nanoparticles. Microelectron Eng. 2012;89:129–32. https://doi.org/10.1016/j.mee.2011.03.149.
35. Sangeetha R, Muthukumaran S, Ashokkumar M. Structural, optical, dielectric and antibacterial studies of Mn doped $Zn_{0.96}Cu_{0.04}O$ nanoparticles. Spectrochim Acta Part A Mol Biomol Spectrosc. 2015;144:1–7.
36. Vegard L. Die Konstitution der Mischkristalle und die Raumfüllung der Atome. Z Physik. 1921;5:17–26. https://doi.org/10.1007/BF01349680.
37. Roguai S, Djelloul A. Synthesis and evaluation of the structural, microstructural, optical and magnetic properties of $Zn_{1-x}Co_xO$ thin films grown onto glass substrate by ultrasonic spray pyrolysis. Appl Phys A Mater Sci Process. 2019;125:1–11. https://doi.org/10.1007/s00339-019-3118-3.
38. Bouloudenine M, Viart N, Colis S, Kortus J, Dinia A, Bouloudenine M, et al. Antiferromagnetism in bulk $Zn_{1-x}Co_xO$ magnetic semiconductors prepared by the coprecipitation technique. Appl Phys Lett. 2005;052501:92–5.
39. Srinet G, Sharma S, Kumar M, Anshul A. Structural and optical properties of Mg modified ZnO nanoparticles: An x-ray peak broadening analysis. Phys E Low-Dimensional Syst Nanostructures. 2021;125:114381. https://doi.org/10.1016/j.physe.2020.114381.
40. Hasan Farooqi MM, Srivastava RK. Structural, optical and photoconductivity study of ZnO nanoparticles synthesized by annealing of ZnS nanoparticles. J Alloys Compd. 2017;691:275–86. https://doi.org/10.1016/j.jallcom.2016.08.245.
41. Vijayaprasath G, Murugan R, Palanisamy S, Prabhu NM, Mahalingam T, Hayakawa Y, et al. Role of nickel doping on structural, optical, magnetic properties and antibacterial activity of ZnO nanoparticles. Mater Res Bull. 2016;76:48–61. https://doi.org/10.1016/j.materresbull.2015.11.053.
42 Goswami M. Enhancement of photocatalytic activity of synthesized Cobalt doped Zinc Oxide nanoparticles under visible

light irradiation. Opt Mater (Amst). 2020;109:110400. https://doi.org/10.1016/j.optmat.2020.110400.
43. Wang W, Hui S, Zhang F, Wang X, Zhang S, Yan J, et al. Fabrication and study on magnetic-optical properties of Ni-Doped ZnO nanorod arrays. Micromachines. 2019;10(9):622.
44. Yang J, Li X, Lang J, Yang L, Wei M, Gao M, et al. Synthesis and optical properties of Eu-doped ZnO nanosheets by hydrothermal method. Mater Sci Semicond Process. 2011;14:247–52. https://doi.org/10.1016/j.mssp.2011.04.002.
45. Ahmad I, Shoaib Akhtar M, Ahmed E, Ahmad M, Keller V, Qamar Khan W, et al. Rare earth Co-doped ZnO photocatalysts: Solution combustion synthesis and environmental applications. Sep Purif Technol. 2020;237:116328. https://doi.org/10.1016/j.seppur.2019.116328.
46. Zelekew OA, Aragaw SG, Sabir FK, Andoshe DM, Duma AD, Kuo DH, et al. Green synthesis of Co-doped ZnO via the accumulation of cobalt ion onto Eichhornia crassipes plant tissue and the photocatalytic degradation efficiency under visible light. Mater Res Express. 2021;8(2): 025010.
47. Yang H, Zhang JX, Lin GJ, Xian T, Jiang JL. Preparation, characterization and photocatalytic properties of terbium orthoferrite nanopowder. Adv Powder Technol. 2013;24:242–5. https://doi.org/10.1016/j.apt.2012.06.009.
48. Vindhya PS, Jeyasingh T, Kavitha VT. Dielectric properties of zinc oxide nanoparticles using annona muricata leaf. AIP Conf Proc. 2019;2082: 080005.
49. Madhumitha G, Fowsiya J, Gupta N, Kumar A, Singh M. Green synthesis, characterization and antifungal and photocatalytic activity of Pithecellobium dulce peel–mediated ZnO nanoparticles. J Phys Chem Solids. 2019;127:43–51. https://doi.org/10.1016/j.jpcs.2018.12.005.
50. Sinthiya MAM, Kumaresan N, Ramamurthi K, Sethuraman K. Development of pure rutile TiO_2 and Magneli titanium suboxide microstructures over titanium oxide-seeded glass substrates using surfactant-free hydrothermal process. Bull Mater Sci. 2019;42. https://doi.org/10.1007/s12034-019-1791-7
51. Ravichandran AT, Karthick R. Enhanced photoluminescence, structural, morphological and antimicrobial efficacy of Co-doped ZnO nanoparticles prepared by Co-precipitation method. Results Mater. 2020;5:100072. https://doi.org/10.1016/j.rinma.2020.100072.
52 Mahroug A, Hamrit S, Guerbous L. Structural, morphological and optical properties of undoped and Co-doped ZnO thin films prepared by sol – gel process. J Mater Sci: Mater Electron. 2014;25(11):4967–74.
53 Yang Z, Ye Z, Zheng X, Zhao B. Effect of the morphology on the optical properties of ZnO nanostructures. Phys E Low-dimensional Syst Nanostructures. 2009;42:116–9. https://doi.org/10.1016/j.physe.2009.09.010.
54. Abirami N, Arulanantham AMS, Wilson KSJ. Structural and magnetic properties of cobalt doped ZnO thin films deposited by cost effective nebulizer spray pyrolysis technique. Mater Res Express. 2020;7(2): 026405.
55. Yong X, Schoonen MAA. The absolute energy positions of conduction and valence bands of selected semiconducting minerals. Am Mineral. 2000;85:543–56.
56. Senol SD, Ozugurlu E, Arda L. Synthesis, structure and optical properties of (Mn/Cu) Co-doped ZnO nanoparticles. J Alloys Compd. 2020;822:153514. https://doi.org/10.1016/j.jallcom.2019.153514.
57. Vindhya PS, Kavitha VT. Comparative study of antibacterial activity of zinc oxide and copper oxide nanoparticles synthesized by green method. AIP Conference Proceedings 2021; 2369:020195. http://aip.scitation.org/doi/abs/10.1063/5.0060909
58. Fiedot-Toboła M, Ciesielska M, Maliszewska I, Rac-Rumijowska O, Suchorska-Wo P, Teterycz H, et al. Deposition of zinc oxide on different polymer textiles and their antibacterial properties. Materials. 2018;11(5):707.
59. Iqbal Y, Raouf Malik A, Iqbal T, Hammad Aziz M, Ahmed F, Abolaban FA, et al. Green synthesis of ZnO and Ag-doped ZnO nanoparticles using Azadirachta indica leaves: Characterization and their potential antibacterial, antidiabetic, and wound-healing activities. Mater Lett. 2021;305:130671. https://doi.org/10.1016/j.matlet.2021.130671.
60. Shankar S, Rhim J. Facile approach for large-scale production of metal and metal oxide nanoparticles and preparation of antibacterial cotton pads Running Title : Preparation of antimicrobial cotton pad. Carbohydr Polym. 2017;163:137–45. https://doi.org/10.1016/j.carbpol.2017.01.059.
61 Pradeev raj K, Sadaiyandi K, Kennedy A, Sagadevan S, Chowdhury ZZ, Johan MRBin, et al. Influence of Mg doping on ZnO nanoparticles for enhanced photocatalytic evaluation and antibacterial analysis. Nanoscale Res Lett. 2018;13(1):1–13.
62 Hojjati-najafabadi A, Davar F, Enteshari Z. Antibacterial and photocatalytic behaviour of green synthesis of $Zn_{0.95}Ag_{0.05}O$ nanoparticles using herbal medicine extract. Ceram Int. 2021;47(22):31617–24. https://doi.org/10.1016/j.ceramint.2021.08.042.
63. Hanif A, Lee I, Akter J, Islam A, Zahid AASM, Sapkota KP, et al. Enhanced photocatalytic and antibacterial performance of ZnO nanoparticles prepared by an efficient thermolysis method. Catalysis. 2019;9(7):608.
64. Harifi T, Montazer M. Application of nanotech- nology in sports clothing and flooring for enhanced sport activities, performance, efficiency and comfort: a review. J Ind Text. 2017;46(5):1147–69.
65. Khan SA, Noreen F, Kanwal S, Hussain G. Comparative synthesis, characterization of Cu-doped ZnO nanoparticles and their antioxidant, antibacterial, antifungal and photocatalytic dye degradation activities. Dig J Nanomater Biostructures. 2017;12:877–89.
66. Ceo G, Naidi SN, Tan AL. Green-synthesized CeO_2 nanoparticles for photocatalytic, antimicrobial, antioxidant and cytotoxicity activities. R Soc Chem. 2021;5599–620.
67. Bharathi D, Bhuvaneshwari V. Synthesis of zinc oxide nanoparticles (ZnO NPs) using pure bioflavonoid rutin and their biomedical applications: antibacterial, antioxidant and cytotoxic activities. Res Chem Intermed. 2019;45:2065–78. https://doi.org/10.1007/s11164-018-03717-9.
68. Nandhakumar E, Priya P, Selvakumar P, Vaishnavi E, Sasikumar A, Senthilkumar N. One step hydrothermal green approach of CuO/Ag nanocomposites : analysis of structural, biological activities. Mater Res Express. 2019;6(9): 095036.
69. Bhatti MA, Tahira A, Chandio Adad, Almani KF, Bhatti AL, Waryani B, et al. Enzymes and phytochemicals from neem extract robustly tuned the photocatalytic activity of ZnO for the degradation of malachite green (MG) in aqueous media. Res Chem Intermed. 2021;47:1581–99. https://doi.org/10.1007/s11164-020-04391-6.
70. Munawar T, Nadeem MS, Mukhtar F, Hasan M, Mahmood K, Arshad MI, et al. Rare earth metal co-doped $Zn_{0.9}La_{0.05}M_{0.05}O$ (M = Yb, Sm, Nd) nanocrystals; energy gap tailoring, structural, photocatalytic and antibacterial studies. Mater Sci Semicond Process. 2021;122:105485.
71. Viswanathan B. Photocatalytic degradation of dyes: An overview. Curr Catal. 2017;7:99–121.
72. Mulmi DDAS, Bhattarai R, Thapa RAMB, Koju R, Nakarmi MIMLAL. Enhanced photocatalytic degradation of organic pollutants by lysozyme-mediated zinc oxide nanoparticles. Bull Mater Sci. 2022;45(2):10. https://doi.org/10.1007/s12034-022-02657-w.
73. Khataee A, Vahid B, Akbarpour A, Aber S. Effect of dye chemical structure on the efficiency of photoassisted electrochemical degradation using a cathode containing carbon nanotubes and a Ti/RuO_2 anode. Res Chem Intermed. 2015;41:6073–85. https://doi.org/10.1007/s11164-014-1723-5.

74. Shuga T, Elsayed H, Mohamed A, Maaza M. ZnO nanoparticles prepared via a green synthesis approach: Physical properties, photocatalytic and antibacterial activity Journal of Physics and Chemistry of Solids ZnO nanoparticles prepared via a green synthesis approach : Physical properties, photoc. J Phys Chem Solids. 2021;160:110313. https://doi.org/10.1016/j.jpcs.2021.110313.
75. El Nemr A, Helmy ET, Gomaa EA, Eldafrawy S, Mousa M. Photocatalytic and biological activities of undoped and doped TiO_2 prepared by Green method for water treatment. J Environ Chem Eng. 2019;7:103385. https://doi.org/10.1016/j.jece.2019.103385.
76. Ahmad W, Singh V, Ahmed S, Nur-e-Alam M. A comprehensive study on antibacterial antioxidant and photocatalytic activity of achyranthes aspera mediated biosynthesized Fe2O3 nanoparticles. Results Eng. 2022;14:100450. https://doi.org/10.1016/j.rineng.2022.100450.
77. Vindhya PS, Kavitha VT. Leaf extract - mediated synthesis of Mn - doped CuO nanoparticles for antimicrobial, antioxidant and photocatalytic applications. Chem Pap. 2022. https://doi.org/10.1007/s11696-022-02631-0.
78 Yakout SM. Robust ferromagnetism and active visible-near infrared photocatalytic properties: Fe based Mn, Co and Ni codoped CuO nanostructures. Opt Mater (Amst). 2021;112:110769. https://doi.org/10.1016/j.optmat.2020.110769.
79. Kannadasan N, Shanmugam N, Cholan S, Sathishkumar K, Viruthagiri G, Poonguzhali R. The effect of Ce^{4+} incorporation on structural, morphological and photocatalytic characters of ZnO nanoparticles. Mater Charact. 2014;97:37–46. https://doi.org/10.1016/j.matchar.2014.08.021.
80. Vasantharaj S, Sathiyavimal S, Senthilkumar P, Kalpana VN, Rajalakshmi G, Alsehli M, et al. Enhanced photocatalytic degradation of water pollutants using bio-green synthesis of zinc oxide nanoparticles (ZnO NPs). J Environ Chem Eng. 2021;9:105772. https://doi.org/10.1016/j.jece.2021.105772.